*Desalination and Water Treatment*
www.deswater.com

doi:10.5004/dwt.2019.23970

153 (2019) 392–401
June

# Degradation of amoxicillin by persulfate activated with $Fe_3O_4$/GO nanocomposite in aqueous solution

Noushin Osouleddini[a], Leila Tajik[b,*], Masoud Moradi[c]

[a]*Department of Chemistry, Ardabil Branch, Islamic Azad University, Ardabil, Iran, Tel. +989906866151, email: Osouleddini.n@gmail.com (N. Osouleddini)*
[b]*Department of Environmental Engineering, Faculty of Environment and Energy, Science and Research Branch, Islamic Azad University, Tehran, Iran, Tel. +989127928511, email: L_tajic441@yahoo.com (L. Tajik)*
[c]*Research Center for Environmental Determinants of Health (RCEDH), Health institute, Kermanshah University of Medical Sciences, Kermanshah, Iran, Tel. +989183859910, email: mahfooz60@gmail.com (M. Moradi)*

Received 13 September 2018; Accepted 17 February 2019

**ABSTRACT**

Entrance of antibiotics to aquatic solution causes the adverse effect on environmental and human health. In this work, $Fe_3O_4$/GO was applied as persulfate (PS) activator to degradation of amoxicillin (AMX). The $Fe_3O_4$/GO nanocomposite was successfully synthesized and characterized by SEM, TEM, XRD, FTIR, BET and XPS analysis. The effects of pH, nanocomposite dosage, GO content, AMX concentration and PS concentration were investigated. Results indicated the AMX degradation was decreased by increasing of pH. The maximum efficiency (100%) was obtained in catalyst dosage (100 mg/L), PS concentration (100 mg/L), AMX concentrations (75 mg/L) and GO content (1:2). It could be concluded that $Fe_3O_4$/GO nanocomposite is the effective activator of PS which has a proper efficiency in the wide range of pH.

*Keywords:* Amoxicillin; Persulfate; $Fe_3O_4$/GO nanocomposite

## 1. Introduction

Amoxicillin is one of the β-lactam antibiotics that widely used in medicine and veterinary to treat bacterial infections [1]. More than 65% of all antibiotics in worldwide are β-lactam group antibiotics (penicillin, amoxicillin and ampicillin) [2]. 32.3% of antibiotics which are used in Iran belong to β-lactam group and amoxicillin is most widely used one [3]. Approximately 30–90% of antibiotics are not metabolized in the human body, and their residual are excreted through urine and stools of humans or animals to the sewage system and eventually water resources [4].Therefore, remarkable amounts of antibiotics have been reported in aquatic environments [5]. Consumption of water containing antibiotic causes acute and chronic toxicity in humans, in addition, antibiotics increase the resistance of pathogens in aquatic environments [6]. Also, sewage containing amoxicillin is often a high TOC wastewater, low biodegradability, and high amount of organic solvents and high soluble salts as well as high odor and color [7]. Many biological and physicochemical methods have been used to remove antibiotics. Biological treatment of antibiotics is not very effective because of the inactivation of effective microorganisms by antibiotics [8]. Therefore, it is necessary to development of effective techniques for the removal of antibiotics. Advanced methods include ozonation, Fenton and photo-Fenton, electrochemical, electron radiation, nanofiltration, chemical coagulation and adsorption processes are the common techniques for contaminants removal [9–13].In comparison with other methods, advanced oxidation process (AOPs) has the most potential to further eliminate resistance contaminants (pharmaceuticals) due to the formation of reactive radicals [14]. Hence, this method is a strong technique to mineralizing organic pollutants into water and carbon dioxide [15]. Oxidation with PS has many advantages over other AOPs (e.g. Fenton), including no need to

*Corresponding author.

low pH, sulfate radical have more potential than oxidation of organic matter in comparison with hydroxyl radical ($HOS_5^- / SO_4^{\cdot-} = +1.82V, H_2O_2 / H_2O = +1.76V$). In addition, PS radical compared to hydroxyl radical acts more selectively in organic matter oxidation [16]. Many methods have been used for activating PS in previous studies, including heat [17], ultrasound [18], UV [19], metal ions such as cobalt and copper [20], zero-valent iron [21], pyrite [22], carbon nanotubes [23], graphene [24].

Using of mentioned methods are limited due to the need for energy, the entry of metal ions into aqueous environments, immunity, sludge production, low activation of PS. In recent years, the use of graphene oxide has grown dramatically due to its unique properties in AOPs [25]. Also, Magnetite ($Fe_3O_4$) nanoparticles have been used for eliminating pollutants and producing nanocomposites due to their magnetic properties, effectiveness, low cost and non-toxicity [26]. Moreover, $Fe_3O_4$ through both ferrous and ferric ions in the environment leads to the easy transfer of electrons and increased catalytic efficiency [27]. Previous studies have shown that iron-containing compositions have been used extensively to activate PS due to the cost-effectiveness, proper activation and no threat to the environment. Iron ions according to Eq. (1) generate sulfate radicals [28].

$$S_2O_8^{2-} + Fe^{2+} \rightarrow SO_4^{\cdot-} + SO_4^{2-} + Fe^{3+} \quad (1)$$

The study of Yan et al. revealed that the sulfamonomethoxine was complete degraded in the presence of $S_2O_8^{2-}$ (1.2 mmol $L^{-1}$) and $Fe_3O_4$ (2.4 mmol $L^{-1}$) [29]. Also, study of Tan et al. indicated that 75% of 10 mg/L acetaminophen was decomposed in the presence of 0.8 g/L $Fe_3O_4$ and 0.2 mM peroxymonosulfate [30]. Generally, $Fe_3O_4$ nanoparticles used instead of $Fe^{2+}$ to activate PS through breaking the oxygen band (O–O bond). This provides the successive use of the $Fe_3O_4$ nanoparticle for re-activation of persulfate [28]. Moreover, due to relatively easy access and easy separation (no secondary contamination) of $Fe_3O_4$, it is introduced as environmental friendly catalyst. Nevertheless, the activation of $Fe_3O_4$ is limited due to its low catalytic activity which leads to incomplete organic compounds degradation [31]. Therefore, combining of $Fe_3O_4$ with graphene oxide, in addition to facilitating its separation, increases the activation of PS. Therefore, in this study $Fe_3O_4$/graphene oxide nanocomposite was synthesized and used to remove of amoxicillin in the presence of PS.

## 2. Materials and methods

### 2.1. Materials

Graphite powder (150–200 mesh), sodium nitrate($NaNO_3$), iron(III) chloride hexahydrate ($FeCl{\cdot}6H_2O$), iron(II) chloride tetrahydrate ($FeCl_2{\cdot}4H_2O$), sulfuric acid ($H_2SO_4$), hydrochloric acid (HCl), potassium permanganate ($KMnO_4$), and hydrogen peroxide ($H_2O_2$) were purchased from Merck, Germany and used without any purification. AMX (CAS 26787-78-0) and Sodium persulfate ($Na_2S_2O_8$ 98%) were purchased from Sigma-Aldrich.pH adjustment was conducted using 0.1 M NaOH and 0.1 M $H_2SO_4$ solutions.

### 2.2. Synthesis of graphene oxide (GO)

GO was synthesized from natural graphite powder via the modified Hummers' method. First, 1.5 g of graphite, 1.5 g of sodium nitrate and 70 mL of sulfuric acid (98%) were mixed together and placed in an ice bath for 2 h. The obtained mixture was heated until 40°C and stirred for 1 h. After that, 100 mL of distilled water were added until temperature was reached 90°C. Then 300 mL of distilled water and 10 mL of hydrogen peroxide were added to mixture. The obtained mixture was then filtered and washed several times with distilled water and diluted hydrochloric acid. Finally, the mixture was separated by centrifugation at 10,000 rpm [32].

### 2.3. Synthesis of $Fe_3O_4$/GO nanocomposites

$Fe_3O_4$/GO was synthesized via combination of co precipitation and thermal methods in the presence of graphene oxide. First, a 100 mL solution was produced containing 4 mM of $FeCl_3{\cdot}6H_2O$ and 2 mM of $FeCl_2{\cdot}4H_2O$ (Ferric/Ferrous molar ratio of 1: 2) at pH = 1.48. Then the pH was adjusted to 4 by adding drop by drop NaOH. Subsequently, certain amount of GO was added to the solution and was placed on stirrer for 30 min. Obtained mixture was transferred to Teflon lined stainless-steel autoclave (200 mL) at 120°C for 10 h. After cooling at ambient temperature, the suspension was filtered and the $Fe_3O_4$/GO composite was obtained. The $Fe_3O_4$/GO composite was rinsed several times by deionized water to remove residual NaOH and then placed in vacuo at 60°C for 24 h [33].

### 2.4. Characteristicsof magnetic graphene oxide (MGO)

The scanning electron microscopy (SEM) (MIRA3, Tescan, Czech Republic) at 5 keV and transmission electron microscopy (TEM) (PHILIPS, TEM) at 100 keV were used for determining the morphologies of GO and $Fe_3O_4$/GO. The information of structural was obtained by X-ray diffraction (XRD) (D8 Advance, Bruker, Germany). Functional groups present in the composite were determined using Fourier transform infrared spectrophotometer (FTIR) (Tensor 27, Bruker, Germany). The nanocomposite surface area was identified by N2 adsorption–desorption isotherms at 77 K with a Bel apparatus (model: Belsorp-mini II, Japan) according to the Brunauer–Emmett–Teller (BET) model. The composition of nanocomposite was determined by X-ray photoelectron spectroscopy (XPS) (K-Alpha+, USA).

### 2.5. Analytical methods

The experiments were carried out in a conical flasks sealed with Teflon-lined screw caps at ambient temperature on stirrer 200 rpm. For this purpose, $Fe_3O_4$/GO catalyst in 2.5–15 mg was added to 100 mL flasks and completely was dispersed by ultrasound. AMX (25–125 mg/L) was then added and was placed on the stirrer. The adsorption and desorption were reached at 20 min. After that, the residual concentration in the AMX solution was measured and considered as the initial concentration. The AMX decomposition process was performed immediately after adding $Na_2S_2O_8$ at concentrations of 25 to 125 mg/L at pH 4, 7 and 9.pH was adjusted by NaOH and $H_2SO_4$ 0.1 M. Then, at a

different time, 2 mL of the sample was taken and passed through a filter (0.22 µm). Also, the $Na_2SO_3$ (0.2 mM) was used to neutralize persulfate and hydroxyl radicals [34]. Amoxicillin was measured by HPLC (CE4100, CECIL, England). Chromatography measurements on HICHROM column with specification HI-5C18-4371, dimensions (200 mm × 4.6 mm). The catalyst was collected and separated in all samples by centrifugation. The samples were filtrated of Syringe (0.22 µm) and then transferred to a HPLC. Methanol and distilled water were used as mobile phase A and B. 0–1 min 100% A; 1–10 min 25% A; 10–15 min 25% A; 15–20 min 100% A. The flow of carrier phase and injection volume was 1 mL/min and 20 µL respectively. The UV-visible detector was used to measure of amoxicillin at 235 nm in ambient temperature (25 ± 2°C) (Fig. 1) [1].

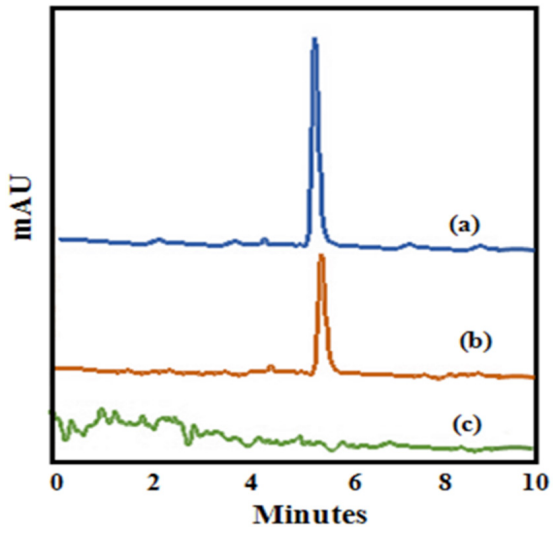


Fig. 1. HPLC-UV chromatogram of AMX at the 235 nm a) before degradation b) after 50% degradation c) after 100% degradation.

## 3. Results and discussion

### 3.1. Nanocomposite characterization

SEM image of the nanocomposite is shown in Fig. 2. As shown, GO surface has irregular clumps cavities. This facilitates the incorporation of $Fe_3O_4$ nanoparticles on the GO surface. As observed $Fe_3O_4$ nanoparticles thickly deposited and irregularly distributed. The TEM image is illustrated in Fig. 3. The morphology of the nanocomposite indicated that $Fe_3O_4$ nanoparticles have been anchored onto the GO sheets and aggregated due to their extremely small size and dipole–dipole coupling, which demonstrated nanocomposite effectually synthesized [35]. The XRD pattern of nanocomposite is shown in Fig. 4. The pattern of GO illustrated the unique peak at $2\theta = 9.98°$ corresponding to GO nanosheets which attributed to (001) plane. The peaks of GO was disappeared after depositing of $Fe_3O_4$ nanoparticles due to the exfoliation of GO layers, less agglomeration of GO sheets in the composite and dominant of robust $Fe_3O_4$ signals on weak signals of carbon [36]. for $Fe_3O_4$/GO,

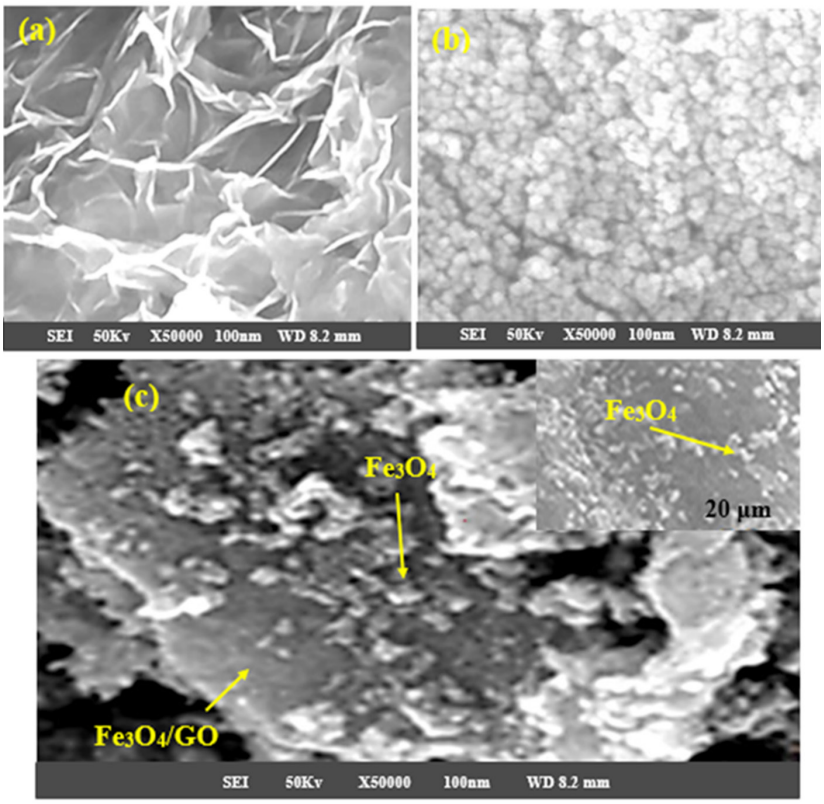


Fig. 2. SEM image of a) GO, b) $Fe_3O_4$, and c) $Fe_3O_4$/GO.

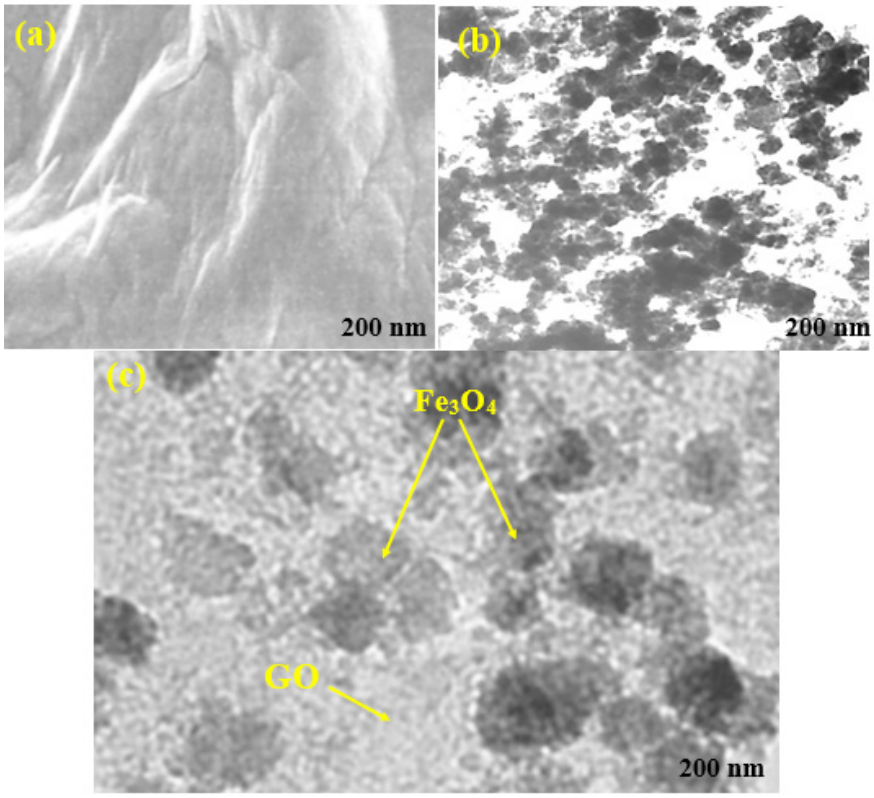


Fig. 3. TEM image of a) GO, b) $Fe_3O_4$ and c) GO.

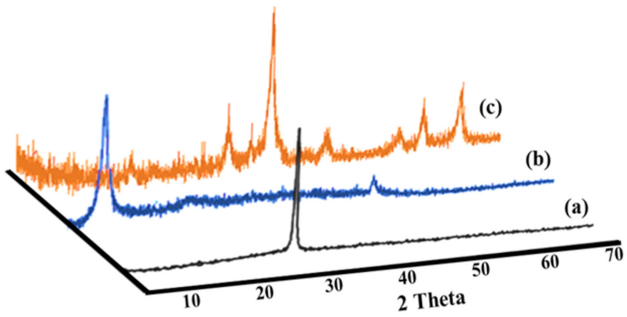


Fig. 4. XRD patterns of a) Graphite b) GO and c) MGO.

the peaks at 2θ = 30.2°, 35.6°, 43.3°, 53.7°, 57.1°, and 62.8° correspond to (220), (331), (400), (422), (511), and (440) are consistent with the standard XRD data for the cubic crystalline structures of $Fe_3O_4$. Moreover, the peaks at 2θ values of 30.2°, 35.6°, 43.3°, and 57.1° are corresponded to maghemite (γ-$Fe_2O_3$) and magnetite ($Fe^{2+}Fe^{3+}{}_2O_4$) and peaks at 2θ = 53.7° and 62.8° related to hematite ($Fe_2O_3$). The peaks at 2θ = 18.2° and 33.1° were corresponded to goethite (α-FeO(OH)) [32].

Fig. 5 shows the FTIR spectra of GO and $Fe_3O_4$/GO. Peaks related to GO were observed at 1380 $cm^{-1}$, 1630 $cm^{-1}$, 1730 and 3270 $cm^{-1}$ assigned to C-OH stretching, C=C stretching mode of the $sp^2$ carbon skeletal network, C=O stretching vibrations and O-H stretching vibration, respectively. For $Fe_3O_4$/GO, three peaks at 1455 $cm^{-1}$, 1533 $cm^{-1}$ and 1647 $cm^{-1}$ appeared which corresponded to amide carbonyl group for $Fe_3O_4$/GO including–CONH amide band I,–NH amide band II and C–N stretch of amide respectively were confirmed the covalent bonding between $Fe_3O_4$ nanoparticles and GO surface [37].

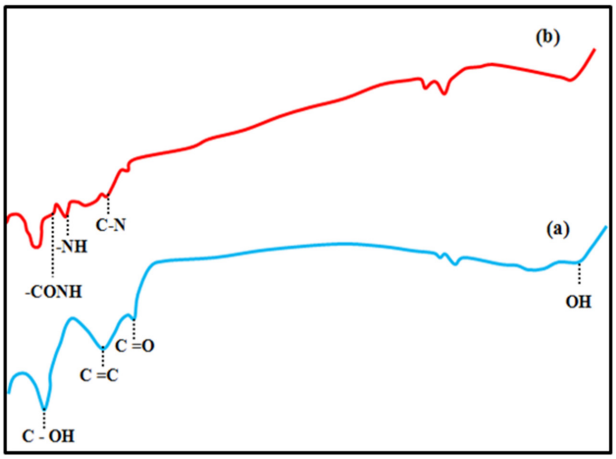


Fig. 5. The FT-IR spectra of a) GO and b) $Fe_3O_4$/GO.

Fig. 6a shows the curve of $N_2$-adsorption-desorption vs. relative pressure for $Fe_3O_4$/GO nanocomposite. The results show that isotherm of $N_2$-adsorption-desorption is as form of type IV shape with $H_2$ hysteresis loop. These results indicate the existence of a mesoporous structure for catalyst. Fig. 6b shows the pore size distribution. As you can

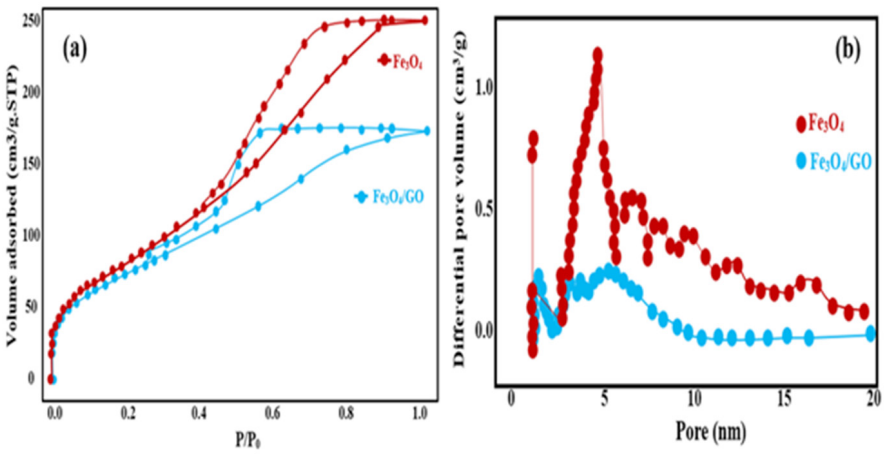


Fig. 6. a) BET adsorption-desorption curve and b) Pore size distribution of $Fe_3O_4$ and $Fe_3O_4$/GO.

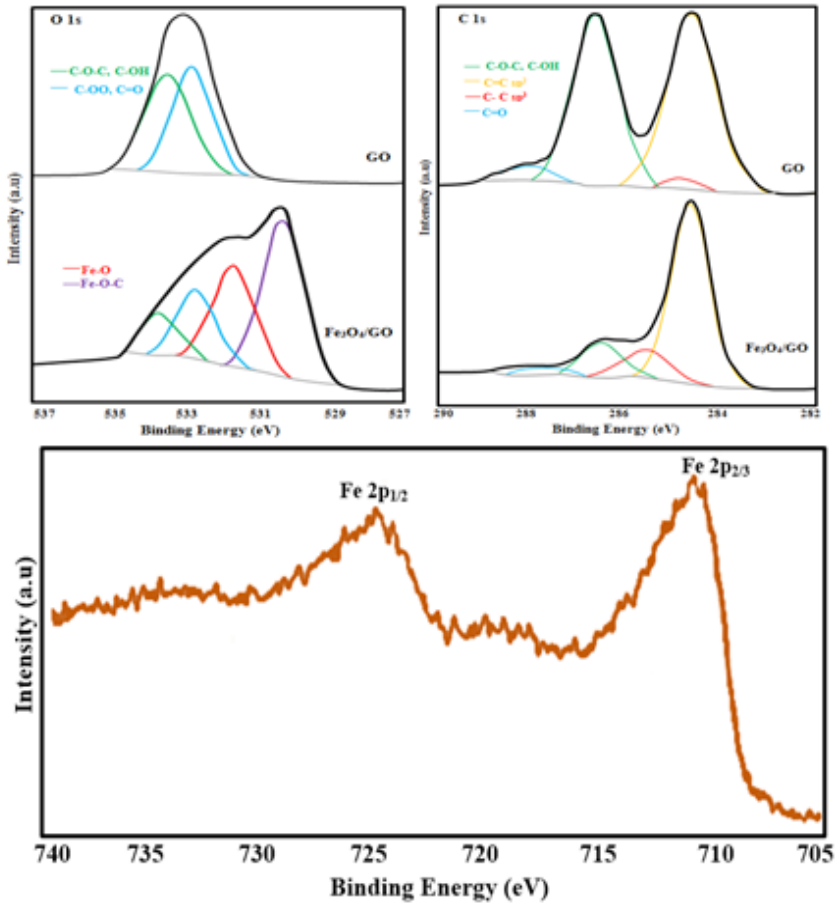


Fig. 7. XPS spectra of GO and $Fe_3O_4$/GO a) O 1s b) C 1s and c) Fe 2p spectra of $Fe_3O_4$/GO.

see, the major peaks are between 3 and 6 nm. According to the Qatari IUPAC recommendation, the mesoporous diameter is between 2 and 50 nm, which is due to the integration of the GO two dimensional structures and the $Fe_3O_4$ zero dimensional structure [38].

Fig. 7a represents the O 1s spectra for $Fe_3O_4$ and $Fe_3O_4$/GO. The results for GO indicate that there are two peaks of 532.2 and 532.9 eV for the oxygen content of the carboxylate/carbonyl group and the epoxy/hydroxyl group, respectively. After the formation of $Fe_3O_4$/GO nanocomposite,

the intensity of the O1s peaks in comparison with the GO decreased and wider, resulting from the oxygen network in the $Fe_3O_4$ nanoparticle (529.9 eV) [39]. Fig. 7b shows the results of the C 1s spectra for GO, which indicates that there are $sp^2$ C = C bands (284.5 eV), carbon in C-OH (286.7 eV) and epoxy/carboxyl C = O (288.1 eV). The results show that carboxylate/carbonyl (C-OH/C-OC) peak in nanocomposite is reduced due to the reaction of iron with carboxylate group (Fe-O-C bonds) [40]. Fig. 7c shows the Fe 2p spectra. As we can see, there are two separate peaks at 711.2 and 725 eV which corresponding to Fe 2p 3/2 and Fe 2p 1/2 in $Fe_3O_4$ nanoparticles, respectively [41].

### 3.2. Effect of pH

pH is one of the important parameters in chemical processes. Fig. 8 shows the effect of pH (4, 7 and 9) on the AMX removal. As observed, the removal of AMX was decreased with increasing of pH, So that the highest efficiency (100%) was obtained at pH = 4. While, with increasing of pH to 7 and 9, the AMX removal was decreased to 83% and 74% respectively. This contributed to negatively charge of PS and activators in neutral and alkali pH which leads to decrease by interaction between $Fe_3O_4$/GO and PS. Moreover, non-radical decomposition of PS increases with increasing pH [42]. While, in the acidic aqueous, more radical persulfates are generated due to acid catalyzation. Hydroxyl ion is also produced at high pH, which acts as a scavenger of persulfate radical [Eq. (2)], thus leads to reducing the efficiency [43].

$$SO_4^- + OH \rightarrow SO_4^{2-} + OH^- \quad (2)$$

On the other hand, in acidic pH, the $H^+$ ions cause the further dissolving of oxide layers on the nanocomposite surface which leads to increase of interaction rate between nanocomposite and PS through more release of ferrous ions and prevents the passivation of the nanocomposite surface [44,45].

$$F_eO_3 + 8H^+ \rightarrow 2Fe^{3+} + Fe^{2+} + 4H_2O \quad (3)$$

In addition, iron ions are more likely to be presenting in divalent in acidic conditions which are more capable of activating PS and radical production compared to trivalent iron ions [46]. The important point about the effect of pH on the removal process is that, despite reducing the removal efficiency at high pH, this efficiency is somewhat high and can effectively eliminate this contaminant. These results indicate the $Fe_3O_4$/GO nanocomposite in the acid-to-alkali range is capable of removing AMX from aqueous solution.

Furthermore, in addition to the effect on surface charge of nanocomposite, pH also, affects on surface charge of nanocomposite, it also, effect on $pK_a$ and solubility of AMX. In our work the $pH_{ZPC}$ of nanocomposite was obtained 6. On the other hand, the $pK_a$ of AMX is 2.67 which indicated the AMX has negative charge in the pH > 2.67. The negative charge of AMX leads to its adsorption on $Fe_3O_4$/GO nanocomposite due to positive charge of nanocomposite at pH < 6. Therefore, the removal efficiency was increased until pH = 4 and then decreased. The reason of efficiency decreasing is due to low solubility of amoxicillin in the pH = 4–6 which cause the limited access of sulfate radicals to the AMX.

### 3.3. Effect of $Fe_3O_4$/GO nanocomposite dosage

The effect of nanocomposite dosage (25–150 mg/L) on the AMX degradation was investigated at AMX concentration (100 mg/L), pH = 4, contact time (150 min) and PS concentration of 100 mg/L (Fig. 9). The results showed that in the absence of $Fe_3O_4$/GO, only 8.4% of amoxicillin decomposed which indicates the low oxidation potential of PS alone. Results showed that the removal efficiency of AMX was increased by increasing the catalyst dosage. So that the 50% removal of AMX was obtained for 25 mg/L, 50 mg/L, 100 mg/L and 150 mg/L catalyst dosages at 90 min, 48 min,

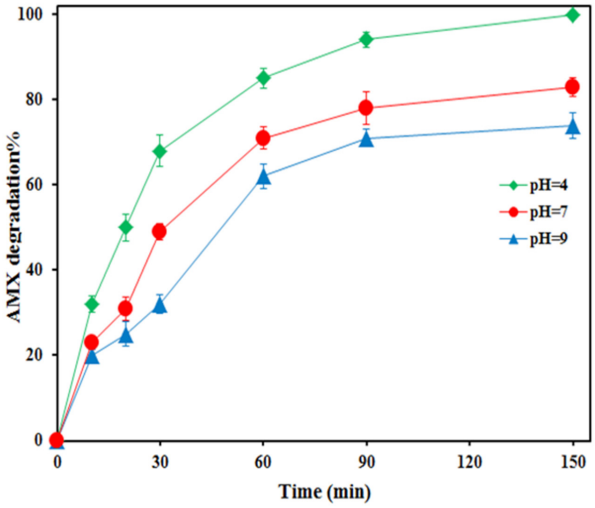


Fig. 8. Effect of pH solution on the AMX degradation ($Fe_3O_4$/GO dosage: 100 mg/L, GO content: 1:2, PS concentration: 100 mg/L, AMX concentration: 75 mg/L).

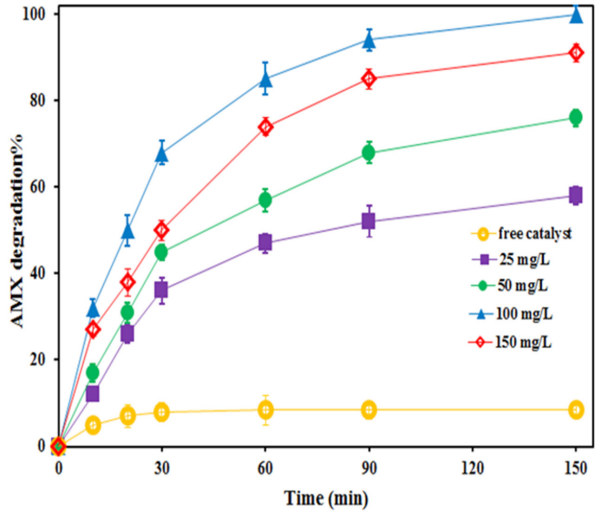


Fig. 9. Effect of nanocomposite dosage on the AMX degradation (pH: 4, GO content: 1:2, PS concentration: 100 mg/L, AMX concentration: 75 mg/L).

20 min and 32 min respectively. This contributed to increase of $Fe_3O_4$/GO nanocomposite sites for PS activation.

$$\equiv Fe(III) + PS \rightarrow \equiv Fe(II) + SO_5^{\bullet -} + H^+ \quad (4)$$

$$\equiv Fe(II) + PS \rightarrow \equiv Fe(III) + SO_4^{\bullet -} + OH^- \quad (5)$$

However, the removal efficiency was reduced with increasing catalyst dosage (150 mg/L). This corresponded to increase of quenching reaction between ferrous ions of nanocomposite and $SO_4^-$ [47].

$$SO_4^- + Fe^{2+} \rightarrow SO_4^{2-} + Fe^{3+} \quad (6)$$

On the other hand, when the dose of a nanoparticle increases by a certain amount, although, production of $SO_4^-$ are increased, but these radicals without reaction to AMX due to reaction with each other are quench [48].

$$SO_4^- + SO_4^- \rightarrow S_2O_8^{2-} \quad (7)$$

Moreover, the self-binding phenomenon is occurred by increasing of nanocomposite dosage which leads to more aggregation of particles and decrease active sites of the catalyst [48].

### 3.4. Kinetics of PS degradation

The PS degradation process in the presence of different doses of $Fe_3O_4$/GO nanocomposite was studied through first-order kinetics, the equation of which is presented below [48].

$$\ln\left[\frac{C}{C_0}\right] = -K_{app}t \quad (8)$$

where $C_0$ and $K_{app}$ are the initial concentration of PS and apparent rate coefficient of degradation ($min^{-1}$), respectively. Therefore, $K_{app}$ will be calculated by the slope of the line derived from $\ln\frac{C}{C_0}$ vs. time. The results showed that PS degradation rate increased up to 0.015 $min^{-1}$ with increasing dose of nanocomposite up to 100 mg/L. This increase in PS degradation is due to its reaction with active sites of nanocomposite, which leads to the degradation of PS into sulfate radicals. However, with further increase in catalyst dosage, ferrous ions react with them due to the production of more radical sulfate, and the PS degradation decreases [Eq. (6)]. Also, in high amounts of sulfate radicals, the quench phenomenon occurs and is converted to PS again [Eq. (7)]

### 3.5. Effect of GO content

Fig. 11 shows the effect of various $Fe_3O_4$/GO ratios (1:0, 1:1, 1:2 and 1:3) on the AMX removal. As shown, the efficiency of removing AMX by $Fe_3O_4$ (1:0) was low and removal efficiency was obtained 65% over a 150 min. While, with increasing GO content up to 1:2 ratio, the removal efficiency was obtained 100% in 150 min. This could be due to activation of PS by GO. Duan et al. revealed that intact $sp^2$-conjugated p system of carbon can generate and hydroxyl radical through dissociation of PMS [49].

On the other hand, AMX degradation was decreased by further increase in the GO ratio (1:3). This contributed to decrease in the amount of $Fe_3O_4$ active sites, thus reducing its catalytic effect on PS activation. On the other hand, the ability of nanocomposite was reduced to activation of PS by increasing the GO ratio due to lack of proper distribution of $Fe_3O_4$ and the aggregation phenomenon [50].

Also, the results display that the $Fe_3O_4$ nanoparticle is the main factor in the activation of persulfate and GO alone has an insignificant role in the activation of persulfate. The reason for issue is that $Fe_3O_4$ by releasing ferrous ions, causes the production of radical hydroxyl [Eq. (5)], then the radical sulfate reacts with AMX and decomposes it [Eqs. (9)–(11)] [51]. Meanwhile, GO alone activates the persulfate

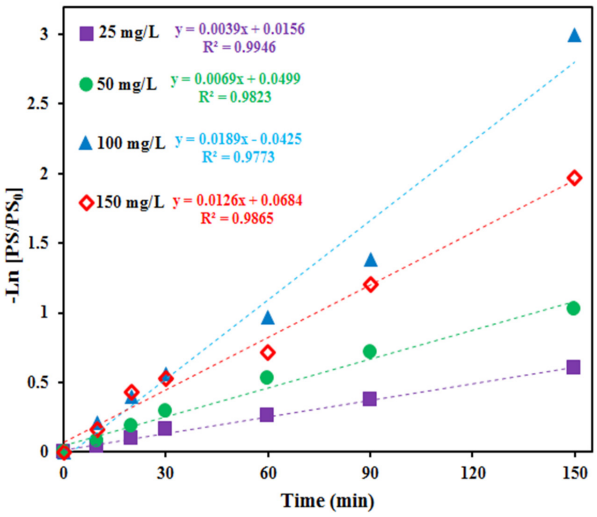


Fig. 10. PS decomposition rate (pH: 4, GO content: 1:2, PS concentration: 100 mg/L, nanocomposite dosage (25–150 mg/L)).

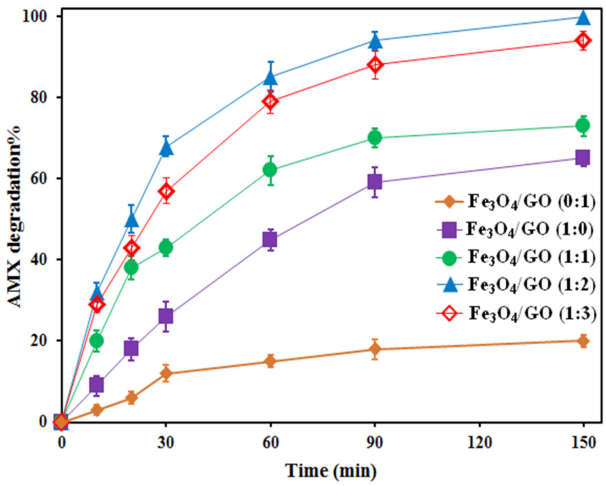


Fig. 11. Effect of GO content on the AMX degradation (pH: 4, nanocomposite dosage: 100 mg/L, PS concentration: 100 mg/L, AMX concentration: 75 mg/L).

via honeycomb-shaped covalent carbon, which does not suffice for activation [52].

$$AMX + SO_4^- \rightarrow SO_4^{2-} + AMX^{\bullet+} \quad (9)$$

$$AMX^{\bullet+} + H_2O \rightarrow (OH)AMX + H^+ \quad (10)$$

$$(OH)AMX \rightarrow \text{Intermediates} \rightarrow\rightarrow CO_2 + H_2O \quad (11)$$

### 3.6. Effect of AMX concentration

The removal efficiency was investigated at different concentrations of AMX (25–125 mg/L) (Fig. 12). Results showed AMX degradation was increased up to 75 mg/L (100%) and then decreased (76% for 125 mg/L). This corresponded to lack of access to reactive radicals at low concentrations of AMX, on the other hand, removal efficiency was decreased in high concentration of AMX due to generation of resistance byproduct. Moreover, the high amount of oxidizing the agent is needed to effectively eliminate of high AMX concentrations [27].

### 3.7. Effect of PS concentration

The concentration of oxidant is one of the important parameters in the removal of contaminants (Fig. 13). Results revealed that AMX degradation was increased at higher concentrations of oxidants due to increased production of free radicals. So that the removal of AMX increased up to 100 mg/L of oxidant and then decreased. This assigned to the interaction between $SO_4^-$ radicals with each other which cause them to be neutralized. Furthermore, there are side reactions between $SO_4^-$ and PS ions that cause the consumption of $SO_4^-$ radicals [52].

$$SO_4^- + SO_4^- \rightarrow S_2O_8^{2-} \quad (12)$$

$$SO_4^- + S_2O_8^{2-} \rightarrow S_2O_8^- + SO_4^{2-} \quad (13)$$

The comparison of the AMX degradation results of this study with the literature is presented in Table 1. As can be observed, regardless of the UV role, the removal efficiency of other PS activator was partly less than the $Fe_3O_4$/GO nanocomposite at the same PS concentration, while, the present study emphasized that it would not use UV due to complexity of operation, risks, high cost and etc.

### 3.8. Reusability of nanocomposite

The reusability of $Fe_3O_4$/GO nanocomposite was conducted by the AMX degradation in five times. The catalyst was washed thoroughly by water before each oxidation run and separated by external magnetic. After each cycle the removal efficiency was calculated and leached Fe was determined by inductively coupled plasma (ICP) (Model: DV-Optima 2100). Results revealed that the removal efficiency was decreased 11% after 5 cycles. The leached Fe indicated the nanocomposite has proper stability (Fig. 14).

## 4. Conclusion

Combining $Fe_3O_4$ and GO is a proper technique for activation of PS to AMX degradation. In this work, nanocomposite was successfully synthesized and characterize by SEM, TEM, XRD, FTIR, BET and XPS analysis. The effect of pH, nanocomposite dosage, GO content, AMX concentration and PS concentration were investigated. Results revealed that $Fe_3O_4$/GO could effectively activate the PS to degrade AMX. The maximum degradation of AMX was obtained in acidic pH. The removal efficiency was increased by increasing the catalyst dosage (up to 100 mg/L), AMX concentrations (up to 75 mg/L) and PS concentrations (up to 100 mg/L). Also, AMX degradation increased by GO content up to 1:2 ratio. Totally, PS, $Fe_3O_4$ and GO individually have low ability to AMX degradation. While, $Fe_3O_4$/GO nanocomposite due to synergistic effect of GO on $Fe_3O_4$ properties could effectively activated PS to AMX degradation in wide range of pH.

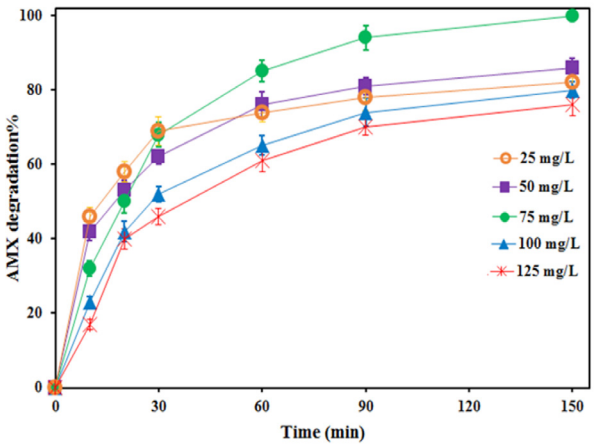


Fig. 12. Effect of AMX concentration on the AMX degradation (pH: 4, nanocomposite dosage: 100 mg/L, GO content: 1:2, PS concentration: 100 mg/L).

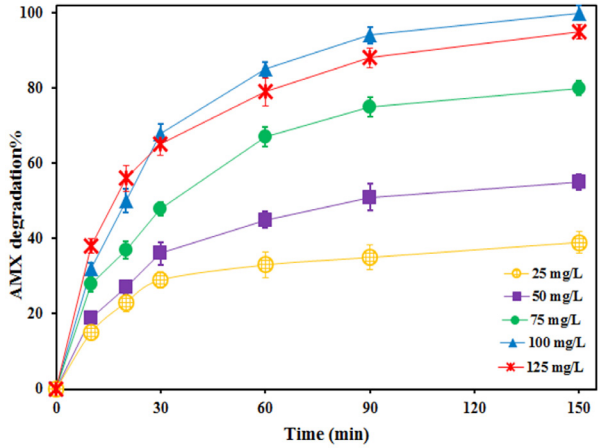


Fig. 13. Effect of PS concentration on the AMX degradation (pH: 4, nanocomposite dosage: 100 mg/L, GO content: 1:2, AMX concentration: 75 mg/L).

Table 1
The comparison of the AMX degradation results of this study with the literature

| S. No | PS activator | PS conc. | pH | Time (min) | β-lactam antibiotics | Removal % | Ref. |
|---|---|---|---|---|---|---|---|
| 1 | UV/$FeS_2$ | 3.5 mM | 3 | 60 | AMX | 93 | 1 |
| 2 | UVC | 40 µM | 6.5 | 120 | AMX | 85 | 2 |
| | UVC//$Fe^{2+}$ | | | | | 95 | |
| 3 | Electro-generated magnetite ($Fe_3O_4$) | 0.08 M | 7 | 60 | AMX | 72.6 | 27 |
| 4 | $Co_3O_4$ | 0.01 M | 6 | 45 | AMX | 91.01 | 54 |
| 5 | UV | 1 mM | 3 | 60 | Ampicillin | 75.6 | 55 |
| 6 | | | | | Cephalothin | 90.7 | |
| 8 | $Fe_3O_4$/GO | 100 mg/L | 4 | 150 | AMX | 100 | Present study |

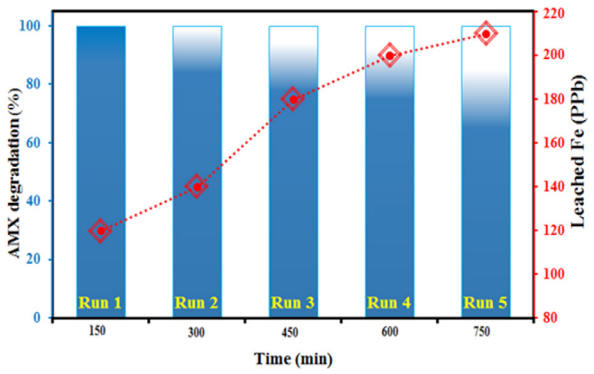


Fig. 14. The AMX degradation using $Fe_3O_4$/GO and leached Fe in five successive cycles.

## Acknowledgements

The authors gratefully acknowledge the Islamic Azad University of Ardabil, (Ardabil, Iran) for the financial support.

## References

[1] R.R. Kalantary, M. Rahmatinia, M. Moradi, Data on modeling of UV/$Na_2S_2O_8$/$FeS_2$ process in amoxicillin removal using Box-Behnken methodology, Data in Brief, 19 (2018) 1810–1815.
[2] E. Kattel, B. Kaur, M. Trapido, N. Dulova, Persulfate-based photodegradation of a beta-lactam antibiotic amoxicillin in various water matrices, Environ. Technol., (2018) 1–9.
[3] A. Mohammadi, M. Kazemipour, H. Ranjbar, R.B. Walker, M. Ansari, Amoxicillin removal from aqueous media using multi-walled carbon nanotubes, Fullerenes, Fuller. Nanotub. Car. N., 23 (2015) 165–169.
[4] R. Andreozzi, M. Canterino, R. Marotta, N. Paxeus, Antibiotic removal from wastewaters: the ozonation of amoxicillin, J. Hazard. Mater., 122 (2005) 243–250.
[5] N. Olama, M. Dehghani, M. Malakootian, The removal of amoxicillin from aquatic solutions using the $TiO_2$/UV-C nano-photocatalytic method doped with trivalent iron, Appl. Water. Sci., 8 (2018) 97.
[6] K. Yaghmaeian, G. Moussavi, A. Alahabadi, Removal of amoxicillin from contaminated water using $NH_4Cl$-activated carbon: Continuous flow fixed-bed adsorption and catalytic ozonation regeneration, Chem. Eng. J., 236 (2014) 538–544.
[7] R. Kıdak, Ş. Doğan, Medium-high frequency ultrasound and ozone based advanced oxidation for amoxicillin removal in water, Ultrason. Sonochem., 40 (2018) 131–139.
[8] A. Boukhelkhal, O. Benkortbi, M. Hamadache, N. Ghalem, S. Hanini, A. Amrane, Adsorptive removal of amoxicillin from wastewater using wheat grains: equilibrium, kinetic, thermodynamic studies and mass transfer, Desal. Water Treat., 57 (2016) 27035–27047.
[9] Y. Vasseghian, E.N. Dragoi, Modeling and optimization of acid blue 193 removal by UV and peroxydisulfate process, J. Environ. Eng., 144 (2018) 06018003.
[10] K. Sharafi, M. Pirsaheb, V.K. Gupta, S. Agarwal, M. Moradi, Y. Vasseghian, E.N. Dragoi, Phenol adsorption on scoria stone as adsorbent-application of response surface method and artificial neural networks, J. Mol. Liq., 274 (2018) 699–714.
[11] M. Moradi, A.M. Mansouri, N. Azizi, J. Amini, K. Karimi, K. Sharafi, Adsorptive removal of phenol from aqueous solutions by copper (cu)-modified scoria powder: process modeling and kinetic evaluation, Desal. Water Treat., 57 (2016) 11820–11834.
[12] M. Moradi, M. Heydari, M. Darvishmotevalli, K. Karimyan, V.K. Gupta, Y. Vasseghian, H. Sharafi, Kinetic and modeling data on phenol removal by iron-modified scoria powder (FSP) from aqueous solutions, Data in Brief, 20 (2018) 957–968.
[13] M. Moradi, M. Soltanian, M. Pirsaheb, K. Sharafi, S. Soltanian, A. Mozafari, The efficiency study of pumice powder to lead removal from the aquatic environment: isotherms and kinetics of the reaction, J. Mazand. Univ. Med. Sci. (JMUMS), 23 (2014) 64–75.
[14] M. Moradi, M. Fazlzadehdavil, M. Pirsaheb, Y. Mansouri, T. Khosravi, K. Sharafi, Response surface methodology (RSM) and its application for optimization of ammonium ions removal from aqueous solutions by pumice as a natural and low cost adsorbent, Arch. Environ. Prot., 42 (2016) 33–43.
[15] H. Arfaeinia, H. Rezaei, K. Sharafi, M. Moradi, H. Pasalari, S. Hashemi, Application of ozone/magnetic graphene oxide for degradation of diazinon pesticide from aqueous solutions, Desal. Water Treat., 107 (2018) 127–135.
[16] S. Su, W. Guo, C. Yi, Y. Leng, Z. Ma, Degradation of amoxicillin in aqueous solution using sulphate radicals under ultrasound irradiation, Ultrason. Sonochem., 19 (2012) 469–474.
[17] C. Tan, N. Gao, Y. Deng, L. Li, J. Deng, S. Zhou, Kinetic oxidation of antipyrine in heat-activated persulfate, Desal. Water Treat., 53 (2015) 263–271.
[18] B. Li, L. Li, K. Lin, W. Zhang, S. Lu, Q. Luo, Removal of 1, 1, 1-trichloroethane from aqueous solution by a sono-activated persulfate process, Ultrason. Sonochem., 20 (2013) 855–863.
[19] Y.Q. Gao, N.Y. Gao, Y. Deng, D.Q. Yin, Y.S. Zhang, Degradation of florfenicol in water by UV/$Na_2S_2O_8$ process, Environ. Sci. Pollut. Res., 22 (2015) 8693–8701.
[20] M. Zhang, X. Chen, H. Zhou, M. Murugananthan, Y. Zhang, Degradation of p-nitrophenol by heat and metal ions co-activated persulfate, Chem. Eng. J., 264 (2015) 39–47.
[21] X. Xiong, B. Sun, J. Zhang, N. Gao, J. Shen, J. Li, X. Guan, Activating persulfate by Fe0 coupling with weak magnetic field: performance and mechanism, Water Res., 62 (2014) 53–62.
[22] C. Liang, Y.Y. Guo, Y.C. Chien, Y.J. Wu, Oxidative degradation of MTBE by pyrite-activated persulfate: proposed reaction pathways, Ind. Eng. Chem. Res., 49 (2010) 8858–8864.

[23] H. Lee, H.J. Lee, J. Jeong, J. Lee, N.B. Park, C. Lee, Activation of persulfates by carbon nanotubes: Oxidation of organic compounds by nonradical mechanism, Chem. Eng. J., 266 (2015) 28–33.
[24] H. Chen, K.C. Carroll, Metal-free catalysis of persulfate activation and organic-pollutant degradation by nitrogen-doped graphene and aminated graphene, Environ. Pollut., 215 (2016) 96–102.
[25] X. Duan, H. Sun, S. Wang, Metal-free carbocatalysis in advanced oxidation reactions, Acc. Chem. Res., 51 (2018) 678–687.
[26] A. Ahmad, X. Gu, L. Li, S. Lv, Y. Xu, X. Guo, Efficient degradation of trichloroethylene in water using persulfate activated by reduced graphene oxide-iron nanocomposite, Environ. Sci. Pollut. Res., 22 (2015) 17876–17885.
[27] F. Sepyani, R.D.C. Soltani, S. Jorfi, H. Godini, M. Safari, Implementation of continuously electro-generated $Fe_3O_4$ nanoparticles for activation of persulfate to decompose amoxicillin antibiotic in aquatic media: $UV_{254}$ and ultrasound intensification, J. Environ. Manage., 224 (2018) 315–326.
[28] J. Yan, Y. Chen, L. Qian, W. Gao, D. Ouyang, M. Chen, Heterogeneously catalyzed persulfate with a CuMgFe layered double hydroxide for the degradation of ethylbenzene, J. Hazard. Mater., 338 (2017) 372–380.
[29] J. Yan, M. Lei, L. Zhu, M.N. Anjum, J. Zou, H. Tang, Degradation of sulfamonomethoxine with $Fe_3O_4$ magnetic nanoparticles as heterogeneous activator of persulfate, J. Hazard. Mater., 186 (2011) 1398–1404.
[30] C. Tan, N. Gao, Y. Deng, J. Deng, S. Zhou, J. Li, X. Xin, Radical induced degradation of acetaminophen with $Fe_3O_4$ magnetic nanoparticles as heterogeneous activator of peroxymonosulfate, J. Hazard. Mater., 276 (2014) 452–460.
[31] X.B. Gong, Degradation of dye wastewater by persulfate activated with $Fe_3O_4$/grapheme nanocomposite, J. Water. Reuse. Desal., 6 (2016) 553–561.
[32] R.R. Kalantary, A. Azari, A. Esrafili, K. Yaghmaeian, M. Moradi, K. Sharafi, The survey of Malathion removal using magnetic graphene oxide nanocomposite as a novel adsorbent: thermodynamics, isotherms, and kinetic study, Desal. Water Treat., 57 (2016) 28460–28473.
[33] L. Yu, J. Chen, Z. Liang, W. Xu, L. Chen, D. Ye, Degradation of phenol using $Fe_3O_4$-GO nanocomposite as a heterogeneous photo-Fenton catalyst, Sep. Purif. Technol., 171 (2016) 80–87.
[34] C. Tan, N. Gao, Y. Deng, J. Deng, S. Zhou, J. Li, X. Xin, Radical induced degradation of acetaminophen with $Fe_3O_4$ magnetic nanoparticles as heterogeneous activator of peroxymonosulfate, J. Hazard. Mater., 276 (2014) 452–460.
[35] J. Hur, J. Shin, J. Yoo, Y.-S. Seo, Competitive adsorption of metals onto magnetic graphene oxide: comparison with other carbonaceous adsorbents, Sci. World. J., 2015 (2015).
[36] G. Xie, P. Xi, H. Liu, F. Chen, L. Huang, Y. Shi, F. Hou, Z. Zeng, C. Shao, J. Wang, A facile chemical method to produce superparamagnetic graphene oxide–$Fe_3O_4$ hybrid composite and its application in the removal of dyes from aqueous solution, J. Mater. Chem., 22 (2012) 1033–1039.
[37] E. Kazemi, S. Dadfarnia, A.M.H. Shabani, Dispersive solid phase microextraction with magnetic graphene oxide as the sorbent for separation and preconcentration of ultra-trace amounts of gold ions, Talanta, 141 (2015) 273–278.
[38] J. Su, M. Cao, L. Ren, C. Hu, $Fe_3O_4$–graphene nanocomposites with improved lithium storage and magnetism properties, J. Phys. Chem. C., 115 (2011) 14469–14477.
[39] M.A. Farghali, T.A. El-Din, A.M. Al-Enizi, R.M. El-Bahnasawy, Graphene/magnetite nanocomposite for potential environmental application, Int. J. Electrochem. Sci., 10 (2015) 529–537.
[40] Y.L. Dong, H.G. Zhang, Z.U. Rahman, L. Su, X.J. Chen, J. Hu, X.G. Chen, Graphene oxide–$Fe_3O_4$ magnetic nanocomposites with peroxidase-like activity for colorimetric detection of glucose, Nanoscale, 4 (2012) 3969–3976.
[41] J. Lu, X. Jiao, D. Chen, W. Li, Solvothermal synthesis and characterization of $Fe_3O_4$ and γ-$Fe_2O_3$ nanoplates, J. Phys. Chem. C, 113 (2009) 4012–4017.
[42] A. Rastogi, S.R. Al-Abed, D.D. Dionysiou, Sulfate radical-based ferrous–peroxymonosulfate oxidative system for PCBs degradation in aqueous and sediment systems, Appl. Catal. B, 85 (2009) 171–179.
[43] M. Ahmadi, F. Ghanbari, M. Moradi, Photocatalysis assisted by peroxymonosulfate and persulfate for benzotriazole degradation: effect of pH on sulfate and hydroxyl radicals, Wat. Sci. Tech., 72 (2015) 2095–2102.
[44] P. Zhou, J. Zhang, J. Liu, Y. Zhang, J. Liang, Y. Liu, B. Liu, W. Zhang, Degradation of organic contaminants by activated persulfate using zero valent copper in acidic aqueous conditions, RSC Adv., 6 (2016) 99532–99539.
[45] M. Moradi, R.R. Kalantary, A. Esrafili, A.J. Jafari, M. Gholami, Visible light photocatalytic inactivation of Escherichia coli by natural pyrite assisted by oxalate at neutral pH, J. Mol. Liq., 248 (2017) 880–889.
[46] M. Samarghandi, J. Mehralipour, G. Azarin, K. Godini, A. Shabanlo, Decomposition of sodium dodecylbenzene sulfonate surfactant by electro/$Fe^{2+}$-activated persulfate process from aqueous solutions, Global Nest. J., 19 (2017) 115–121.
[47] G.P. Anipsitakis, D.D. Dionysiou, Radical generation by the interaction of transition metals with common oxidants, Environ. Sci. Technol., 38 (2004) 3705–3712.
[48] M. Kermani, F. Mohammadi, B. Kakavandi, A. Esrafili, Z. Rostamifasih, Simultaneous catalytic degradation of 2,4-D and MCPA herbicides using sulfate radical-based heterogeneous oxidation over persulfate activated by natural hematite (α-$Fe_2O_3$/PS), J. Phys. Chem. Solids, 117 (2018) 49–59.
[49] X. Duan, Z. Ao, L. Zhou, H. Sun, G. Wang, S. Wang, Occurrence of radical and nonradical pathways from carbocatalysts for aqueous and nonaqueous catalytic oxidation, Appl. Catal. B Environ., 188 (2016) 98–105.
[50] J. Yan, W. Gao, M. Dong, L. Han, L. Qian, C.P. Nathanail, M. Chen, Degradation of trichloroethylene by activated persulfate using a reduced graphene oxide supported magnetite nanoparticle, Chem. Eng. J., 295 (2016) 309–316.
[51] Y. Jingchun, M. Lei, L. Zhu, M.N. Anjum, J. Zou, H. Tang, Degradation of sulfamonomethoxine with $Fe_3O_4$ magnetic nanoparticles as heterogeneous activator of persulfate, J. Hazard. Mater., 186 (2011) 1398–1404.
[52] C. Hao, K.C. Carroll, Metal-free catalysis of persulfate activation and organic-pollutant degradation by nitrogen-dopedgraphene and aminated grapheme, Environ. Pollut., 215 (2016) 96–102.
[53] A. Ledjeri, I. Yahiaoui, F. Aissani-Benissad, The electro/$Fe^{3+}$/peroxydisulfate (PDS) process coupled to activated sludge culture for the degradation of tetracycline, J. Environ. Manage., 184 (2016) 249–254.
[54] W. Guo, S. Su, C. Yi, Z. Ma, Degradation of antibiotics amoxicillin by $Co_3O_4$-catalyzed peroxymonosulfate system, Environ. Prog. Sustain. Energy, 32 (2013) 193–197.
[55] X. He, S.P. Mezyk, I. Michael, D. Fatta-Kassinos, D. Dionysiou, Degradation kinetics and mechanism of β-lactam antibiotics by the activation of $H_2O_2$ and $Na_2S_2O_8$ under UV-254 nm irradiation, J. Hazard. Mater., 279 (2014) 375–383.